Hindawi
Advances in Civil Engineering
Volume 2019, Article ID 3732982, 8 pages
https://doi.org/10.1155/2019/3732982

Research Article

Stability Analysis and Reinforcement of a High-Steep Rock Slope with Faults: Numerical Analysis and Field Monitoring

Qibing Zhan,[1] **Xinjian Sun**,[1] **Cheng Li**,[2,3] **Yawei Zhao**,[1] **Xinjie Zhou**,[1] **Yinpeng He**,[1] **and Yuxiang Zhang**[1]

[1]*Sanjiangyuan Ecological and Plateau Husbandry National Key Laboratory, Department of Water Conservancy and Electric Power, Qinghai University, Xining, Qinghai 810016, China*
[2]*Key Laboratory for Special Area Highway Engineering of Ministry of Education, School of Highway, Chang'an University, Xi'an, Shannxi 710064, China*
[3]*Research and Development Center of Transport Industry of Technologies, Materials and Equipment of Highway Construction and Maintenance, Gansu Road & Bridge Construction Group, Lanzhou, Gansu 730030, China*

Correspondence should be addressed to Xinjian Sun; sunxj@qhu.edu.cn and Cheng Li; cli@chd.edu.cn

Received 9 January 2019; Revised 28 January 2019; Accepted 12 February 2019; Published 5 March 2019

Academic Editor: Behzad Esmaeili

This study presents a stability analysis of a high-steep rock slope with two faults during excavations and evaluates the effectiveness of a proposed reinforcement method using prestressed anchor cables. A 3D finite difference model was established based on the strength reduction method using FLAC3D software. The influence of various fault conditions and the effectiveness of the reinforcement on the slope stability during the excavation process were analyzed and compared to field monitoring data. The numerical analysis and field monitoring results showed that the fault close to the slope surface (f20) was prone to the local instability under external forces caused by the excavation, but a fault further away from the slope surface (f14) had insignificant influence on the stability of the slope. Based on the numerical analysis results, the proposed reinforcement measure can increase the factor of safety (FOS) of the slope by 19.2%. The field monitoring data also showed that the displacement of the monitoring point gradually decreased after the reinforcement, and the deformation of the slope was effectively controlled.

1. Introduction

Faults or weak intercalations can adversely affect the stability of rock slopes during the construction process and also make the stability analysis become more complicated [1–3]. The slope stability analysis was originally developed based on the analysis of lateral soil pressure and foundation bearing capacity in soil mechanics. Coulomb's method [4] for estimating the lateral soil pressure on retaining walls and Rankine's method [5] for calculating active and passive soil pressures are considered as the origin of the limit equilibrium method of the slope stability analysis. This traditional method has also been continuously improved, including Swedish method [6], Bishop method [7], simplified Janbu method [8], Spencer method [9], Morgenstern–Price method [10], and Sarma method [11]. Since the 1970s, with the rapid development of the computer technology, various numerical analysis methods including finite element, finite difference, and discrete element methods have been proposed and applied to slope stability analyses [12–14], which significantly improved the speed and accuracy of a slope stability analysis. In recent years, the strength reduction method proposed by Zienkiewicz et al. [15] has gradually become to the focus of theoretical research and widely used in engineering projects for slope stability analyses [16–23].

This case study focuses on evaluating how the excavation process can influence the stability of a high-steep rock slope with faults and the effectiveness of the proposed reinforcement method. A 3D finite difference model was

established based on the strength reduction method using FLAC3D software. The movement of the rock slope was monitored during the excavation process and compared to the numerical analysis results.

2. Site Descriptions and Soil Properties

2.1. Site Descriptions. The rock slope is a cutting slope located behind the powerhouse of the Yangqu hydropower station at the Hainan Tibetan Autonomous Prefecture in Qinghai province, China (Figure 1). The height of the slope is 118.6 m, and the elevation at the toe of the slope is 2560.4 m.

The cross-sectional profile of the slope before and after the excavation is shown in Figure 2. The original slope was consisted of four layers: (1) the slope surface was covered with loosened quaternary soil (Q4pl + dl); (2) the second layer was a highly weathered silty slate with 25 to 30 m thickness; (3) the third layer was a layer of moderately weathered sandy slate with phyllite with 15 to 45 m thickness; and (4) the bottom rock below the ground water table (2605 m) was slightly weathered sandy slate.

Based on the site investigation, there were two faults (f14 and f20) existing in the rock slope, and both of the two faults were approximate 50 cm wide filled with crushed rocks and clay. The angles of the f14 and f20 faults were 72° and 75°, respectively (Figure 2). Before the excavation, no landslide or large deformation was observed.

2.2. Mechanical Properties of Rock Mass and Structural Plane. The mechanical properties of representative samples collected from each of the layers and the two faults are summarized in Tables 1 and 2, respectively. The elastic modulus and Poisson's ratio of the samples were measured by uniaxial compression tests, and the cohesion and friction parameters were measured by direct shear tests. The required bulk modulus (K) and shear modulus (G) were calculated based on the measured elastic modulus and Poisson's ratio. The intact rock properties determined using the laboratory tests may be different with those of the rock mass, and some empirical correlations were found in previous studies (e.g., [24]).

3. Numerical Simulation Method

3.1. The Strength Reduction Method. According to the strength reduction method, the FOS of a slope is defined as the ratio between the actual shear strength and the shear strength when the critical failure occurred. When applying the strength reduction method in finite difference models, the gravitational acceleration of the rock and soil is usually considered as a constant. By reducing the cohesion (c) and internal friction angle (φ) of the soils gradually, a new set of shear strength parameters can be generated after dividing both parameters by a reduction factor (F_s), as shown in equations (1) and (2). Based on the Mohr–Coulomb failure criterion, the FOS of the slope is smallest F_s before failure:

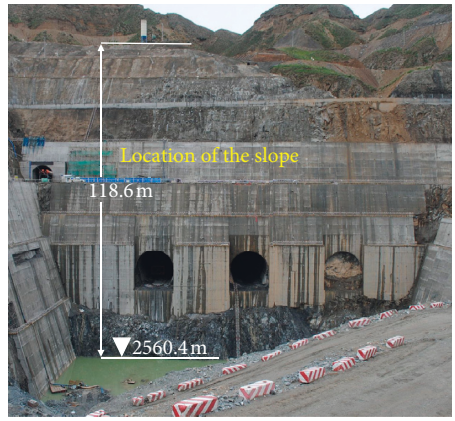

Figure 1: The rock slope of Yangqu hydropower station.

$$c' = \frac{1}{F_s} c, \tag{1}$$

$$\varphi' = \arctan\left(\frac{1}{F_s} \tan \varphi\right). \tag{2}$$

Compared to the traditional slope stability analysis method, the strength reduction method combining with the finite difference method has the following advantages:

(1) Both the constitutive relationships of rock and soil and the effect of deformation on stress are considered in the method

(2) It does not need to assume the shape of the slip surface or to divide the slope into many strips for calculations

(3) Failure processes and actual shape of slip surfaces can be simulated

(4) Support structures and reinforcement can be simulated

3.2. The FLAC3D Model. To explore the influence of the faults on the stability of the slope during excavation, a 3D model was established based on the actual geological conditions to simulate the excavation process, as shown in Figure 3. The simulated slope was 175 meter in length (y-direction), 85 meter in width (x-direction), and 150 meter in height (z-direction), and the tetrahedron mesh was used.

In this study, the rock mass and faults were simulated using 3D solid elements, and the interface between the faults and rock mass was treated as a continuous medium according to [25], and the Mohr–Coulomb plastic model was selected as the constitutive model. In reality, it is possible that the rock mass contains yield regions with the initial stress state. Therefore, the initial stress state of the rock mass was calculated using the elastic-plastic method in each model, which is more reasonable than using the elastic method.

The simulation process was divided into three stages: (1) the cohesive force and tensile strength of the components were set to very large values, and the elastic method

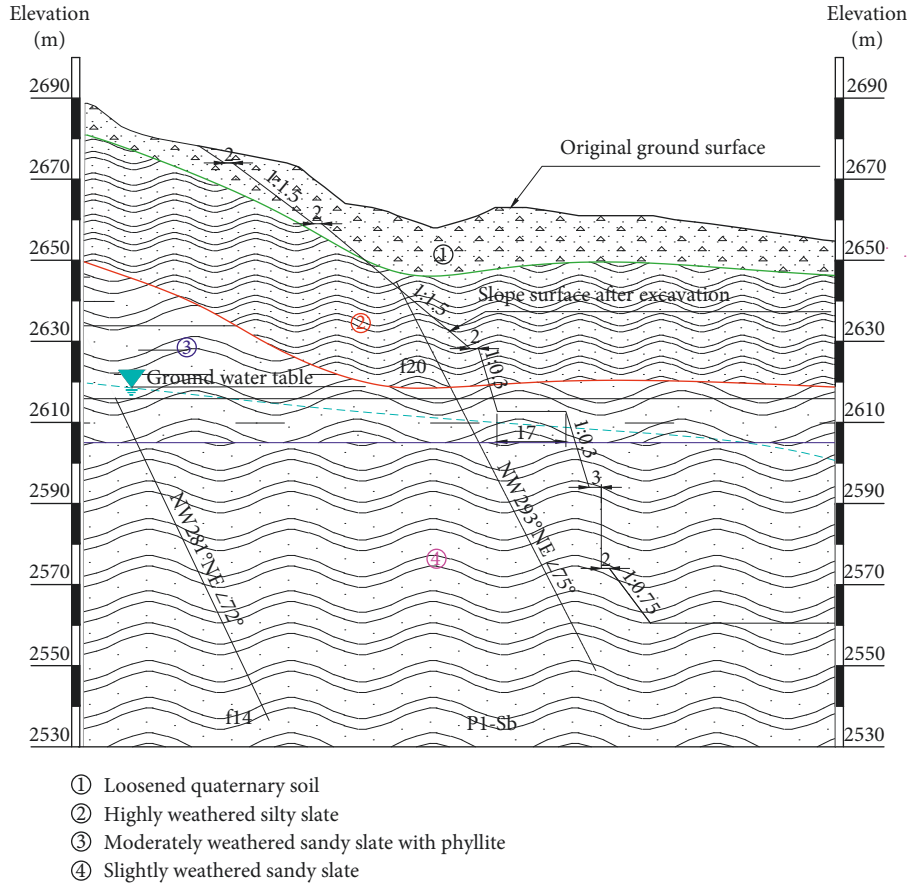

① Loosened quaternary soil
② Highly weathered silty slate
③ Moderately weathered sandy slate with phyllite
④ Slightly weathered sandy slate

Figure 2: Representative geological cross-sectional profile of the slope.

Table 1: Mechanical properties of the intact rock specimens.

Layer no.	Total unit weight, γ (kN/m^3)	Elastic modulus, E (GPa)	Poisson's ratio, μ	Cohesion, c (MPa)	Friction angle, φ (deg.)
①	25.5	0.06	0.32	0.04	28.5
②	26.5	2.00	0.31	0.24	31.5
③	26.8	5.50	0.28	0.45	35.5
④	27	9.00	0.25	0.90	39.5

Table 2: Mechanical properties of the two faults.

Fault no.	Total unit weight, γ (kN/m^3)	Elastic modulus, E (GPa)	Poisson's ratio, μ	Cohesion, c (MPa)	Friction angle, φ (deg.)
Fault f14	26.8	0.45	0.30	0.02	17.5
Fault f20	26.8	0.50	0.29	0.02	17.5

was used for the simulation until the system reaches to the force equilibrium state under gravity; (2) the cohesive force and tensile strength were then reset to initial values to solve the plastic stage until the system reaches to the force equilibrium state; and (3) the velocity and displacement fields of each model were then cleared, and only the stress field was retained. After calculating the initial stress field of each model, the null model in FLAC3D was used to simulate the excavation process, and the elastic-plastic solution of the Mohr–Coulomb constitutive model was used again until the rock mass and faults system reaches to the force equilibrium state.

Four different fault condition combinations were evaluated using the 3D finite difference model, as shown in Table 3.

In the 3D model, the boundary of the X-direction (short edge) and Y-direction (long edge) was restraint in normal direction. While the bottom boundary of the Z-direction was fully constraint, and the top was free. The excavation process was simulated using six stages in the model, as shown in Figure 3.

Three commonly used criteria for determining whether a slope reached to the critical failure state in the numerical analysis are listed below:

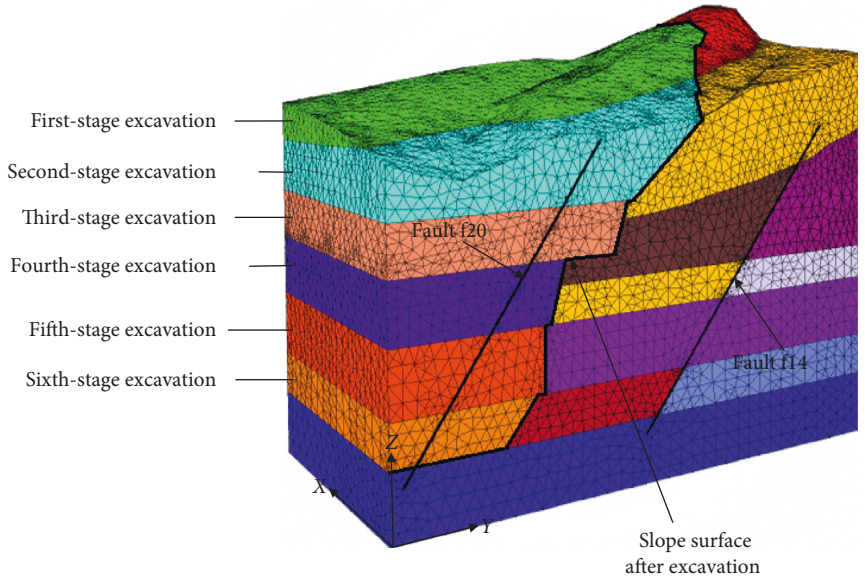

Figure 3: The 3D finite difference model of the rock slope with two faults.

Table 3: Mechanical properties of the rock masses.

Case number	Simulated conditions	Faults
1	No fault	—
2	One fault	f14
3		f20
4	Two faults	f14, f20

(1) *A sudden large displacement observed*: When increasing the reduction factor (F_s), a sudden large displacement of the slope occurred indicating the slope reached to the critical failure state.

(2) *Plastic zone connected*: Due to the elastoplastic behavior of soil and rock masses, the plastic deformation occurs when the stress reaches to a certain level. It is believed that the failure of rock mass is closely related to the expansion of plastic strain zones. If the slope failure occurred, the plastic strain zones have to be connected which will cause the overall instability of the slope.

(3) *The numerical model cannot converge*: When a slope reaches to the critical failure state, a sudden large deformation on the slip surface will occur, so changes of the displacement and strain level will not remain at a constant level, and the numerical model cannot find a solution which can satisfy both the static equilibrium and the stress-strain relationship. Consequently, the static equilibrium equations have no solution, and the numerical model cannot converge.

According to Zhao et al. [26], when a slope reaches to the failure state, neither of the force or displacement can converge. Therefore, they believe that the static equilibrium equations have no solution; so, it can be an indicator of the slope failure. Also, Griffiths and Lane [27] and Dawson et al. [28] concluded that the nonconvergence is a rational sign for a slope failure in numerical analyses. Hence, in this study, the nonconvergence is used as the slope failure criterion.

4. Influences of the Faults on the Slope Stability during Excavation

The numerical analysis results of the four different cases (Table 1) are compared in Figure 4. For all the four cases, the FOS of the slope decreases during the excavation process. For the Cases 1 and 2, changes of the FOS yield similar trends, and the FOS of the slope without a fault is slightly higher than that of the slope with fault f14 during excavation. This phenomenon indicates that the fault f14 further away from the slope surface has little influence on the stability of the slope during the excavation process. Compared to the Cases 1 and 2, the FOS of the Cases 3 and 4 shows greater reduction during the excavation process and significantly decrease after the excavation Stage 5 begun. The comparison results suggest that fault f14 further away from the slope surface has little influence on the stability of the slope, but the fault f20 close to the slope surface can significantly influence the FOS of the slope.

The excavation Stage 1 of the slope was mainly in the Layer 1, so the calculated FOS of the four cases are approximately the same. For the Case 4, the newly formed slope after excavation between the Stages 1 and 2 of the excavation was small; so, the reduction in the FOS was relatively small. From Stage 3 to 5, the high-steep slope was formed, but the numerical analysis results showed relatively small reduction in the FOS, which indicates that the rock mass close to the toe of the slope can prevent the slope from moving downward. However, after the excavation Stage 5 completed, the rock close to the toe of the slope was almost removed, so the FOS significantly reduced from 1.93 to 1.46.

For the Case 4, according to the maximum shear strain increment contour plot after the excavation (Figure 5), the potential failure region of the slope distributed along the

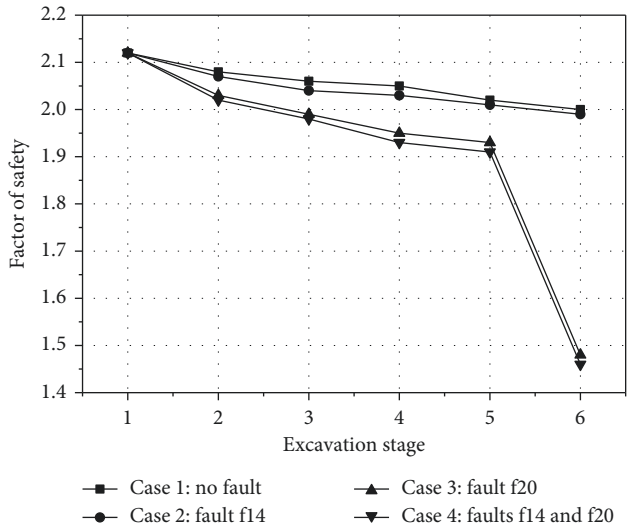

Figure 4: Changes of the FOS of the rock slope with different fault conditions during excavation.

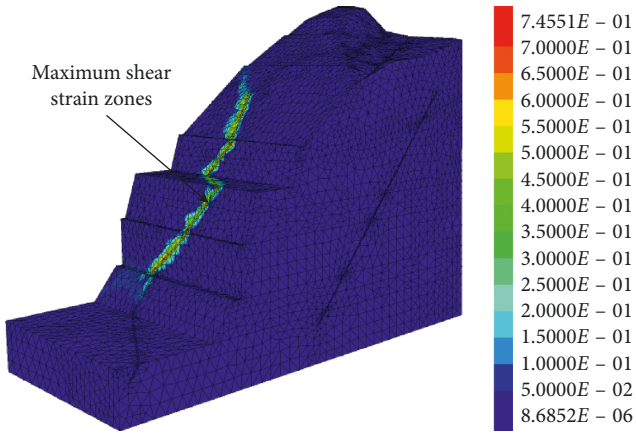

Figure 5: Contour plot of the maximum shear strain after excavation of the slope (Case 4).

fault f20, but there was no potential slip zone around the fault f14. By analyzing the maximum shear strain increment calculation, fault f20 can yield more significant influence on the slope stability during the excavation, which is consistent with the finding derived from the FOS aspect.

5. Effectiveness of the Proposed Reinforcement Method

Although the slope was under the effect of two faults, its FOS still reached to 1.46, which is stronger than the required FOS of the first-grade slope (1.25 to 1.3) under normal operation condition [29]. The exposed area of the fault f20 and the nearby fractured rock mass may have considerable influence on the slope stability under external loads, including construction equipment and disturbances caused by the construction. Therefore, in this study, we proposed using prestressed anchor cables to reinforce the slope, as shown in Figure 6.

To reinforce the fault f20, the 1000 and 2000 kN prestressed anchor cables were installed with 10-degree angle and 4 m by 4 m spacing, as shown in Figure 6. The properties of the prestressed anchorage cable and the grouting materials are listed in Tables 4 and 5, respectively.

The established 3D model was also used to evaluate the effectiveness of the proposed reinforcement method for Case 4 with two faults. The prestress anchor cables were simulated using the cable element in the FLAC3D, and the parameters of the anchorage are set to the maximum value to simulate the tray. The prestress was loaded on the free segment of the cable. Due to the excavation angles of the Stages 1 and 2 were relatively small, no prestressed anchor cable support was installed. For the rest excavation stages, the excavated area was anchored immediately after completing each stage.

To verify the numerical simulation results and also evaluate the effectiveness of the proposed reinforcement method, the calculated displacement results were compared to the field displacement monitoring data collected from the monitoring Point Y9 of slope. The position of the monitoring Point Y9 is shown in Figure 6.

Figure 7 shows the calculated and field monitored downward displacement data of the monitoring Point Y9. It has been found that from June 20 to August 20, 2015, the displacement of the Point Y9 increased by 19.69 mm. According to field construction reports, a local collapse happened on July 7, 2015, at the exposed area of fault f20 from the elevation of 2603 to 2572 m, which resulted in an obvious slope displacement. In the later period, the displacement of the monitoring point kept increasing during the excavation process, because the construction platform was disturbed by external force of the construction traffic and equipment, and the rock mass close to the toe of the slope was removed. The slope displacement reached to 34.59 mm when the excavation of the slope was completed. Several treatments were then applied on the collapse area such as backfilling of microexpansive self-compacting concrete and installing the prestressed anchor cables after the excavation Stages 4 and 5. The monitoring data show that the displacement rate of the monitoring Point Y9 started reducing after the reinforcement. The maximum displacement (35.81 mm) was begun to be monitored on November 4, 2016, and the displacement remained at a relatively constant level. Based on the field monitoring data, the displacement reduced to 22.51 mm (~37%) on February 19, 2018, and there was a trend to further decrease, which indicates the reinforcement measure can effectively improve the stability of the rock slope.

According to the field displacement monitoring data, the maximum displacement value of the slope was 30.48 mm without any reinforcement treatments, while the displacement reduced to 17.63 mm after the reinforcement. The calculated values are slightly smaller than the field monitoring data. This discrepancy may be due to three reasons: (1) the external force disturbance (i.e., construction traffic and equipment) on the platform was not simulated in the numerical analysis, (2) the collapse rock mass around the monitoring Point Y9 was not included in the model, and (3)

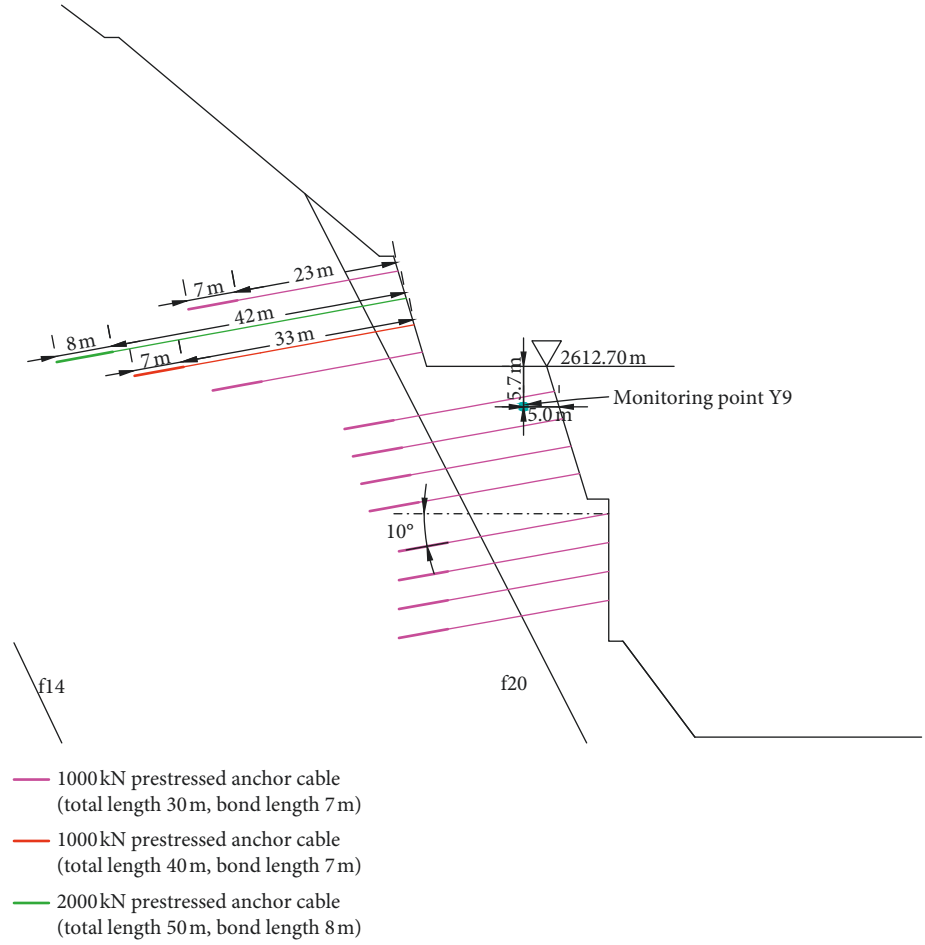

Figure 6: The cross-sectional layout of the prestressed anchorage cables installed in the slope.

Table 4: Parameters of the prestressed anchorage cable.

Parameter	1000 kN	2000 kN
Number of steel strand (bundle)	7	14
Diameter of steel strand (mm)	15.24	15.24
Elastic modulus of steel strand (GPa)	180	180
Nominal section area of steel strand (mm^2)	980	1960
Yield strength of steel strand (MPa)	1860	1860

Table 5: Parameters of the grouting.

Parameter	1000 kN	2000 kN
Stiffness of grouting body (GPa)	15	15
Anchor hole diameter (mm)	120	150
Length of anchorage section (m)	7	8
Cohesion of grouting body (N/m)	1×10^6	1×10^6
Friction of grouting body (deg.)	42	42

the complicated fractured structures of the faults were simplified in the numerical simulation model.

The calculated FOS values of the rock slope with and without the reinforcement are compared in Table 6. Because the anchor cable was installed after the Stage 3 completed, the FOS of the Stages 1 and 2 was the same. The FOS of the Stages 3, 4, and 5 was improved after the reinforcement installed. The FOS of the slope after the excavation Stage 6 increased by 19.2% (from 1.46 to 1.74) with the reinforcement treatment, which indicates that installing the anchorage measure is an efficient way to improve the stability of the rock slope during the excavation process.

6. Summary and Conclusions

In this study, the stability of a high-steep rock slope with two faults during the excavation process and the effectiveness of the proposed reinforcement method were numerically evaluated using the strength reduction method. A 3D finite difference model was established in FLAC3D software to evaluate the influence of various fault combination conditions on the stability of the rock slope during excavation. The FOS of the slope with and without installing the prestressed anchor cables was compared. To verify the numerical simulation results, the calculated displacement data were compared to field displacement monitoring data. Several key findings from this study are summarized below:

(1) Based on the numerical analysis results of the four simulated fault conditions, it has been found that the fault f20 close to the slope surface had more significant influence on the slope stability, while the fault f14 further away from the surface had little influence.

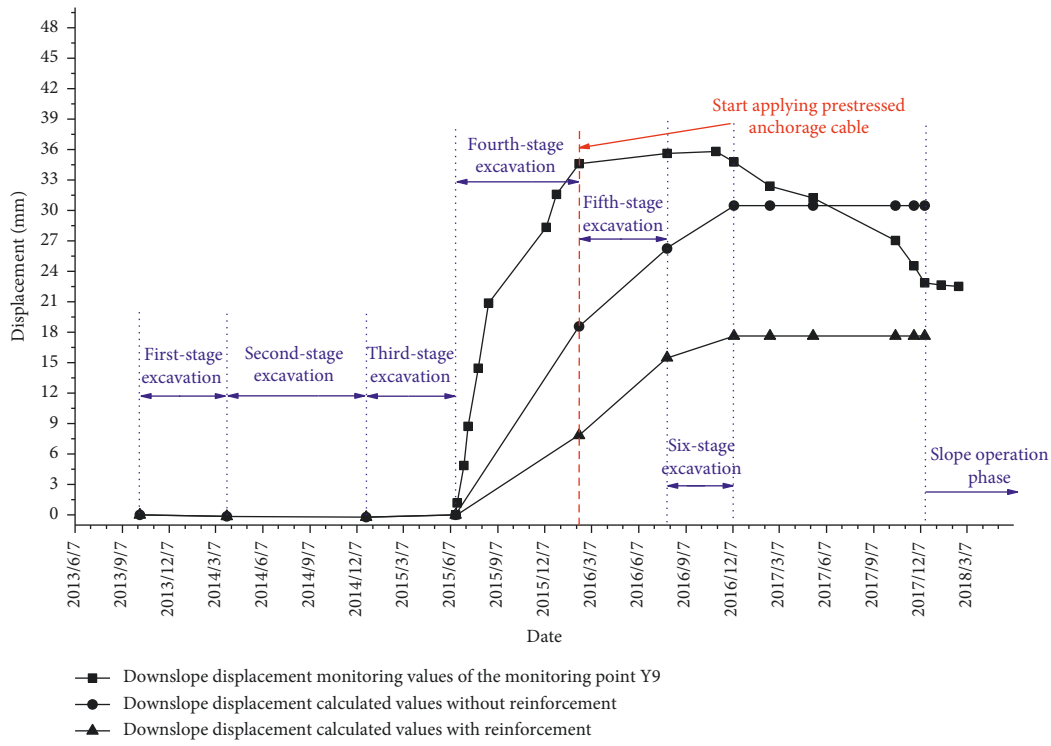

Figure 7: Numerical calculated and field monitored downward displacement data of the monitoring Point Y9 before and after the reinforcement.

Table 6: Calculated FOS values of the rock slope with and without the reinforcement.

Excavation stages	Unreinforced	Reinforced
1	2.12	2.12
2	2.02	2.02
3	1.98	2.09
4	1.93	2.08
5	1.91	2.07
6	1.46	1.74

(2) The numerical analysis results showed that the potential slip surface of the slope is along the fault f20. During the excavation process, the fault f20 and its influenced zone were prone to local instability under external force caused by the construction traffic and equipment loads. This finding was verified by an actual local landslide occurred at the slope surface.

(3) Both the numerical simulation results and field monitoring data showed that the strength reduction method performed well for simulating field conditions, and the proposed reinforcement method of installing the prestressed anchor cables can effectively reduce the downward movement and improve the stability of the rock slope with faults.

Data Availability

The data used to support the findings of this study are available from the corresponding author upon request.

Conflicts of Interest

The authors declare that they have no conflicts of interest.

Acknowledgments

The authors gratefully acknowledge the Fourth Engineering Bureau of China Water Resources and Hydropower Co. Ltd. for providing the field displacement monitoring data and construction reports during the construction of the rock slope. The financial support provided by the Opening Foundation of Research and Development Center of Transport Industry of Technologies, Materials and Equipment of Highway Construction and Maintenance (Gansu Road & Bridge Construction Group) under Grant no. GLKF201804 is also appreciated.

References

[1] Y. Lei, J. N. Hao, and Q. Xiao, "Inquiring some problem in high slope design," *Chinese Journal of Geotechnical Engineering*, vol. 32, no. s2, pp. 610–614, 2010.

[2] D. Stead and A. Wolter, "A critical review of rock slope failure mechanisms: the importance of structural geology," *Journal of Structural Geology*, vol. 74, no. 3, pp. 1–23, 2015.

[3] J. H. Chen, K. Wang, and F. S. Zhong, "Approach and application of rock slopes' stability assessment under the comprehensive effect of multiple factors," *Science and Technology Review*, vol. 31, no. 20, pp. 20–25, 2013.

[4] C. A. Coulomb, "Essai sur une application des règles de maximis et minimis à quelques problèmes de statique relatifs à l'architecture," in *Mémoires de Mathématique et de Physique*

Présentés à l'Académie Royale des Sciences par Divers Savants, et lus Sans ses Assemblées, Vol. 7, Imprimerie Royale, Paris, France, 1776.

[5] W. Rankine, "On the stability of loose earth," *Philosophical Transactions of the Royal Society of London*, vol. 147, pp. 9–27, 1857.

[6] W. Fellenius, *Erdstatische Berechnungen mit Reibung und Kohäsion (Adhäsion) und unter Annahme Kreiszylindrischer Gleitflächen*, Ernst & Sohn, Berlin, Germany, 1927.

[7] A. W. Bishop, "The use of the slip circle in the stability analysis of slopes," *Géotechnique*, vol. 5, no. 1, pp. 7–17, 1955.

[8] N. Janbu, *Slope Stability Computations*, University of Norway, Trondheim, Norway, 1968.

[9] E. Spencer, "A method of analysis of the stability of embankments assuming parallel inter-slice forces," *Géotechnique*, vol. 17, no. 1, pp. 11–26, 1967.

[10] N. R. Morgenstern and V. E. Price, "The analysis of the stability of general slip surfaces," *Géotechnique*, vol. 15, no. 1, pp. 79–93, 1965.

[11] S. K. Sarma, "Stability analysis of embankments and slopes," *Journal of the Geotechnical Engineering Division*, vol. 105, no. 12, pp. 1511–1524, 1979.

[12] S. H. Li, T. P. Liu, and X. Y. Liu, "Analysis method for landslide stability," *Chinese Journal of Rock Mechanics and Engineering*, vol. 28, no. 2, pp. 3309–3324, 2009.

[13] J. M. Duncan, M. Christopher, P. Daniel, and A. P. Miguel, "Slope stability then and now," in *Geo-Congress*, American Society of Civil Engineers, San Diego, CA, USA, 2013.

[14] C. J. Ding, L. H. Zhang, G. R. Yu, and Y. X. Zhang, "Research current situation and development trend of slope stability analysis method," *Water Resources and Power*, vol. 29, no. 8, pp. 112–114, 2011.

[15] O. C. Zienkiewicz, C. Humpheson, and R. W. Lewis, "Associated and non-associated visco-plasticity and plasticity in soil mechanics," *Géotechnique*, vol. 25, no. 4, pp. 671–689, 1975.

[16] Y. R. Zheng and S. Y. Zhao, "Application of strength reduction fem in soil and rock slope," *Chinese Journal of Rock Mechanics and Engineering*, vol. 23, no. 19, pp. 3381–3388, 2004.

[17] P. Marianna and U. Gianfranco, "Analysis of slope-stabilising piles with the shear strength reduction technique," *Computers and Geotechnics*, vol. 102, pp. 238–251, 2018.

[18] Y. Wei, B. Bai, X. C. Li, and H. B. Wang, "A strength reduction method based on double reduction parameters and its application," *Journal of Central South University*, vol. 20, no. 9, pp. 2555–2562, 2013.

[19] F. Guo, Z. Z. Liang, B. Gong, and G. Li, "Tensile failure in stability analysis of rock and soil slopes," *Chinese Journal of Rock Mechanics and Engineering*, vol. a01, pp. 3192–3205, 2017.

[20] J. Shen and M. Karakus, "Three-dimensional numerical analysis for rock slope stability using shear strength reduction method," *Canadian Geotechnical Journal*, vol. 51, no. 2, pp. 164–172, 2014.

[21] F. Tschuchnigg, H. F. Schweiger, and S. W. Sloan, "Slope stability analysis by means of finite element limit analysis and finite element strength reduction techniques. Part II: back analyses of a case history," *Computers and Geotechnics*, vol. 70, pp. 178–189, 2015.

[22] G. Q. Chen, Y. Q. Huang, Y. C. Shi, and Q. Xu, "Stability analysis of slope based on dynamic and whole strength reduction methods," *Chinese Journal of Rock Mechanics and Engineering*, vol. 33, no. 2, pp. 243–256, 2014.

[23] S. H. Jiang, D. Q. Li, X. Y. Di, L. M. Zhang, and C. B. Zhou, "Efficient three-dimensional reliability analysis of anabutment slope at the left bank of Jinping I hydropower station during construction," *Chinese Journal of Rock Mechanics and Engineering*, vol. 34, no. 2, pp. 349–361, 2015.

[24] J. Shen, M. Karakus, and C. Xu, "A comparative study for empirical equations in estimating deformation modulus of rock masses," *Tunnelling and Underground Space Technology*, vol. 32, no. 11, pp. 245–250, 2012.

[25] Y. R. Zheng and L. Kong, *Geotechnical Plastic Mechanics*, China Architecture & Building Press, Beijing, China, 2010.

[26] S. Y. Zhao, Y. R. Zheng, and Y. F. Zhang, "Study on slope failure criterion in strength reduction finite element method," *Rock and Soil Mechanics*, vol. 26, no. 2, pp. 332–336, 2005.

[27] D. V. Griffiths and P. A. Lane, "Slope stability analysis by finite elements," *Geotechnique*, vol. 49, no. 3, pp. 387–403, 1999.

[28] E. M. Dawson, W. H. Roth, and A. Drescher, "Slope stability analysis by strength reduction," *Géotechnique*, vol. 49, no. 6, pp. 835–840, 1999.

[29] Profession Standard of the People's Republic of China, *SL386-2007 Design Code for Engineered Slopes in Water Resources and Hydropower Projects*, China Water Power Press, Beijing, China, 2007.